

# High-speed photography of the development of microdamage in trabecular bone during compression

Philipp J. Thurner,<sup>a)</sup> Blake Erickson, and Zachary Schriock

*Physics Department, University of California–Santa Barbara, Santa Barbara, CA 93106*

John Langan, Jeff Scott, and Maria Zhao

*Computational Sensors Corp., Santa Barbara, California 93103*

James C. Weaver

*Department of Molecular, Cellular and Developmental Biology, University of California–Santa Barbara, Santa Barbara, California 93106*

Georg E. Fantner, Patricia Turner, Johannes H. Kindt, and Georg Schitter

*Physics Department, University of California–Santa Barbara, Santa Barbara, California 93106*

Daniel E. Morse

*Department of Molecular, Cellular and Developmental Biology, University of California–Santa Barbara, Santa Barbara, California 93106*

Paul K. Hansma

*Physics Department, University of California–Santa Barbara, Santa Barbara, California 93106*

(Received 4 October 2005; accepted 31 January 2006)

The mechanical properties of healthy and diseased bone tissue were extensively studied in mechanical tests. Most of this research was motivated by the immense costs of health care and social impacts due to osteoporosis in post-menopausal women and the aged. Osteoporosis results in bone loss and change of trabecular architecture, causing a decrease in bone strength. To address the problem of assessing local failure behavior of bone, we combined mechanical compression testing of trabecular bone samples with high-speed photography. In this exploratory study, we investigated healthy, osteoarthritic, and osteoporotic human vertebral trabecular bone compressed at high strain rates. Apparent strains were found to transfer into a broad range of local strains. Strained trabeculae were seen to whiten with increasing strain. Comparison of whitened regions seen in high-speed photography sequences with scanning electron micrographs showed that the observed whitening was due to the formation of microcracks. From the results of a motion energy filter applied to the recorded movies, we saw that the whitened areas are, presumably, also areas of high deformation. In summary, high-speed photography allows the detection of microdamage in real time, leading toward a better understanding of the local processes involved in bone failure.

## I. INTRODUCTION

Mechanical testing of trabecular bone is a vast experimental field,<sup>1</sup> mainly motivated by the cost and social impact of osteoporosis, a systemic, skeletal disease,<sup>2,3</sup> which leads to a reduction of bone strength and a concomitant increase of fracture risk. Trabecular bone is situated at the end of the long bones and in the spinal column, where it fills all of the inner vertebral space. In the long bones, it transfers loads from joint faces onto the

midshaft of the bone; in lumbar vertebrae, trabecular bone carries and transfers up to 90% of the applied load.<sup>4,5</sup> Thus, a change in trabecular bone quality can have a huge impact on strength and on fracture risk in vertebrae. Standard mechanical tests, however, deliver only integral information on a bone sample and no information regarding local processes experienced in the elastic, yield, and post-yield region. To close this gap, experiments have been devised to combine mechanical testing and imaging of trabecular and cortical bone.<sup>6,7–11</sup> Most of these approaches deliver three-dimensional (3D) information. However, they all are somewhat time-consuming and thus limited to quasi-static testing and/or recording of only a few different states of a sample subjected to mechanical testing. In contrast, high-speed

<sup>a)</sup>Address all correspondence to this author.

e-mail: thurner@physics.ucsb.edu

This paper was selected as the Outstanding Meeting Paper for the 2005 MRS Spring Meeting Symposium L Proceedings, Vol. 874. DOI: 10.1557/JMR.2006.0139

photography is designed to record very fast processes, which allows uncovering in a two-dimensional (2D) fashion the failure dynamics of bone samples subjected to mechanical testing in real time. In this article, we present a novel system consisting of a custom made mechanical testing device and a high-speed camera used to record movies of small bone samples loaded in compression at strain rates around 50%/s. In an exploratory study, we used this system to investigate failure of trabecular bone from healthy, osteoarthritic, and osteoporotic human subjects. During compression, all samples exhibited whitening of strongly deformed trabeculae, which is hypothesized to be due to microcracking.<sup>12</sup> In this paper, we provide experimental evidence proving this hypothesis right. Applying a motion energy filter, we present an example showing correlation between local deformation, as evidenced by detected motion, and whitening. Overall, high-speed photography was found to be useful for delivering results complementary to those of conventional mechanical tests.

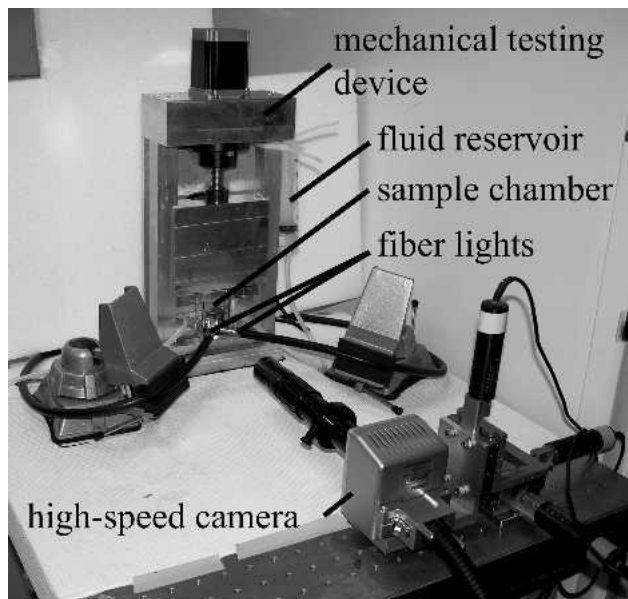
## II. MATERIALS AND METHODS

### A. Sample preparation

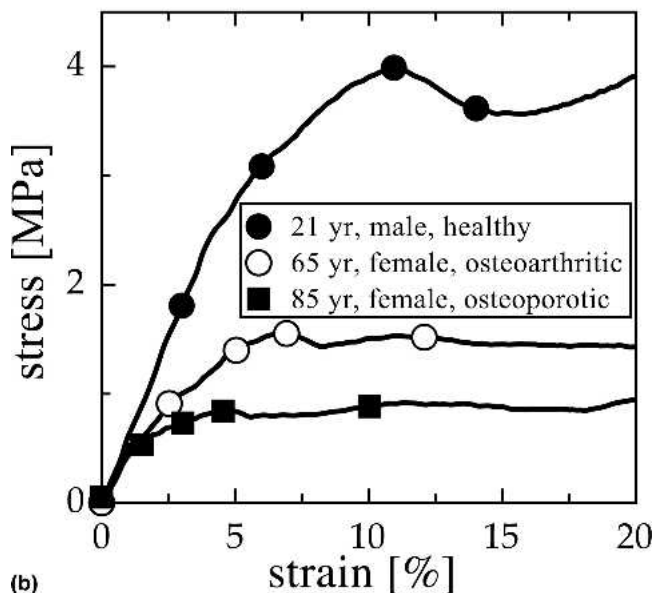
In this study, we investigated bone samples from a previously healthy male donor with no diagnosed bone disease 21 years of age, a female donor 65 years of age, diagnosed with arthritis in her fingers, and a female donor 85 years of age who had suffered from an osteoporotic hip fracture. Cuboid bone samples with a height of 4 mm and cross-sectional dimensions of 4.9 mm by 4.9 mm were cut from thoracic (previously healthy donor) and lumbar (diseased donors) vertebrae using a bandsaw (Marmed Inc. Cleveland, OH) under constant irrigation with water. The smaller sample dimension is oriented parallel to the original principal load bearing direction, i.e., the superior-inferior direction. Bone marrow was extracted from the specimens using a jet of pressurized water.

### B. Mechanical testing

A photograph of the experimental setup, including the high-speed camera system, is given in Fig. 1(a). Compression testing of all samples was done using a custom-made mechanical testing device consisting of a load frame and a piston driven by a stepper motor. The piston impinges onto the transparent sample chamber made from polymethyl methacrylate (PMMA) consisting of a frame and a plunger, which applies the displacement onto the sample. The sample chamber has a fluid inlet and outlet, allowing for immersion of the specimen in fluid. It has to be noted that the sample chamber used in this study had two holes (fluid inlet and outlet) in the plane supporting the lower face of the samples (just below to



(a)



(b)

FIG. 1. (a) Photograph of the experimental setup and (b) stress versus strain curves of the three bone specimens tested in compression.

the two front corners of the samples), leading to a potential underestimation of stress and elastic modulus. In this study, the displacement of the plunger and, from this, the apparent strain, were directly calculated from the recorded high-speed photography frames (see Sec. II. D). The load on the sample was measured with a 250 lb capacity load cell (Model LBC-250, Transducer Techniques Inc., Temecula, CA), which was mounted onto the lower end of the piston. The experiment was controlled using a PC and LabView (National Instruments, Austin, TX). A displacement rate of 2 mm/s was used for all mechanical tests resulting in strain rates around 50%/s. Elastic modulus, yield stress and strain, as well as failure

stress and strain were calculated from the observed stress–strain curves. Failure was defined as the first local maximum of recorded stress after the yield point.

### C. High-speed photography

We used an Ultima 512 high-speed camera (Photron Inc., San Diego, CA) with a pixel resolution of 512 × 512. The camera was equipped with a KC lens, with a KC-AUX and an IF-3 lens mounted on top of it (Infinity, Boulder, CO). The high-speed camera can record up to 32,000 frames/s but has limited memory of 512 MB. We recorded images at a rate of 1000 frames/s and a shutter opening time of 1/8500 s. The scene was illuminated from the front using two fiber lights (MH-100, Dolan Jenner Industries Inc. Lawrence, MA) at angles of about  $\pm 45^\circ$ .

### D. Image processing

For the computation of apparent strains, we measured the size of the plunger in pixels in the different movies and used this as a calibration for the physical size of an image pixel. A texture correlation<sup>13</sup> algorithm was then applied to detect the motion of the plunger. A region of interest with high contrast was selected on the plunger and tracked in subsequent recorded frames. The tracking also allowed synchronization between recorded image data and stress curves. A motion energy filter<sup>14</sup> was applied to a selected region of interest in the high-speed photography movie of the osteoarthritic bone sample, which detects sample motion. Motion energy processing utilizes spatial and temporal filtering to produce an output image sequence where image intensity represents a measure of local scene motion. Prior to motion detection, the dataset was subjected to a spatial frequency filter.

### E. Scanning electron microscopy

For electron microscopy, the samples were transferred in their original configuration to a custom-made aluminum vise and rinsed briefly with water and 95% ethanol to remove residual buffer. Subsequently, they were air dried, further connected to the vise with silver paint, sputtercoated with gold, and imaged with a Vega TS 5130MM SEM (Tescan, Brno, Czech Republic). All images were recorded with an accelerating voltage of 20 keV.

## III. RESULTS

The stress–strain curves retrieved from the compression experiments are shown in Fig. 1(b). The differences in mechanical properties of the three different bone samples are clearly visible. The mechanical parameters derived from the curves are given in Table I. In this preliminary study, most values are observed to decrease progressively from healthy to osteoarthritic and osteoporotic bone. The principal exception is that the elastic modulus is higher for the osteoporotic sample compared to the osteoarthritic one, although this may be a reflection of individual sample variability. In terms of fracture resistance, the energy to failure is of special interest; this is drastically reduced in the diseased specimens, compared to the healthy specimen.

Selected frames from the movies of the samples under compression recorded with the high-speed photography system are given in Fig. 2. The individual frames correspond to the points marked on the stress–strain curves depicted in Fig. 1(b). The frames show that the apparent strain is distributed quite unevenly within the bone samples; some trabeculae are strongly deformed, whereas others seem not to be deformed at all. Strongly deformed trabeculae can be seen to whiten with increasing strain in all samples; however, this effect is more pronounced in the healthy and osteoarthritic bone samples. A magnified detail from the latter is also shown in Fig. 2, where the whitening effect is clearly visible. The magnified detail of the osteoarthritic sample was processed using a motion energy filter to detect absolute and relative motion. The filter was applied in both the  $x$  (left-right) and  $y$  (up-down) direction of the recorded frames. The outcome of the filtering process is a movie containing the detected motion in the different directions over time. Figure 3 shows one frame of the high-speed sequence, the region of interest used for motion filtering as well as the response of the motion energy filter in both directions and a vector plot of the combined motion. For the trabecula that bends to the left and whitens during compression, a clear motion signature in the same direction was detected. The fact that the vector plot in this same area, shown in Fig. 3(e), does not appear uniform is an indication of elevated local strains. A region of interest in another sample from the healthy human donor shown at different strains is presented in Fig. 4. The diagonally oriented trabecula located in the middle of the

TABLE I. Mechanical parameters derived from the recorded stress–strain curves.

Donor	Elastic modulus, $E$ (MPa)	Yield strain, $\epsilon_y$ (%)	Yield stress, $\sigma_y$ (MPa)	Failure strain, $\epsilon_f$ (%)	Failure stress, $\sigma_f$ (MPa)	Energy to failure, $W_f$ (J)
Healthy, male, 21 yr	60.0	4.5	2.6	10.9	4.0	28.4
Osteoarthritic, female, 65 yr	37.7	2.8	1.0	6.9	1.6	6.8
Osteoporotic, female, 85 yr	46.2	1.3	0.5	4.6	0.8	2.7

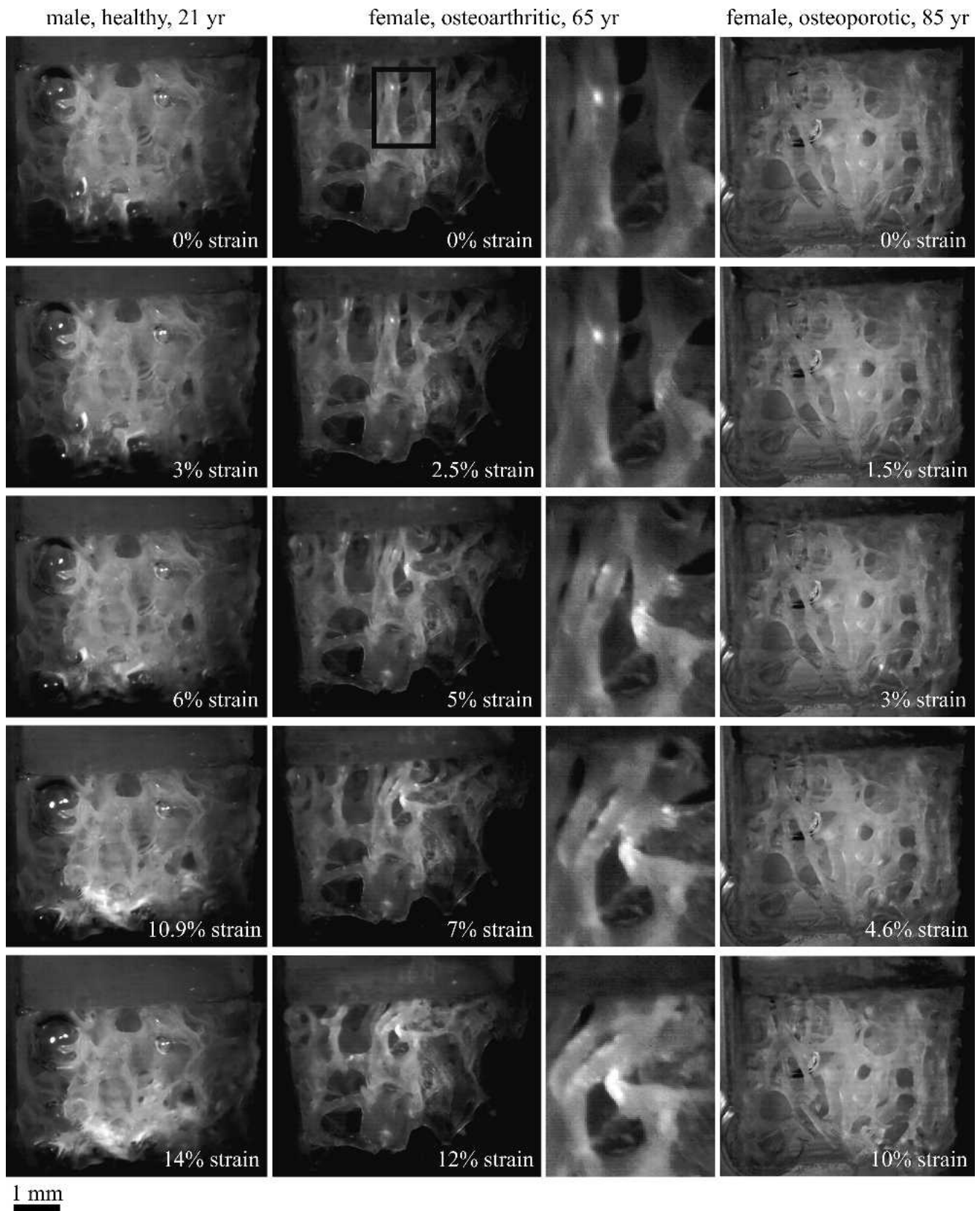


FIG. 2. High-speed photography frames of the bone specimens tested in compression. The frames correspond to the points marked on the stress-strain curves in Fig. 1(b). Trabeculae are seen to whiten with increasing local strain, especially in the case of the healthy and osteoarthritic bone specimens, as can also be seen in the magnified detail of the osteoarthritic bone sample.

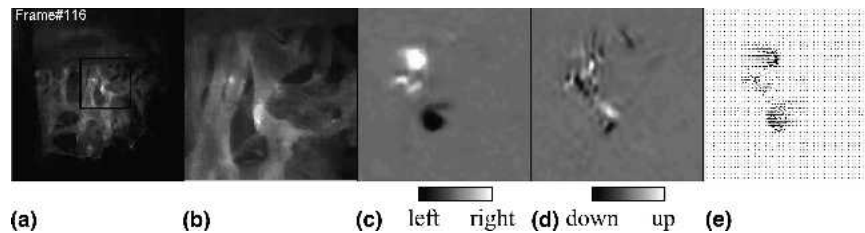


FIG. 3. (a) Frame and (b) magnified detail of the osteoarthritic bone sample under compression. The motion energy filter was applied in two directions: (c) horizontal and (d) vertical. (e) The combined motion vectors are also given.

individual images starts to whiten around an apparent strain of 4%, close to the yield strain of 4.2% of this sample, and the whitening increases with increasing strain. After compression testing the sample was harvested for scanning electron microscope (SEM) investigation. In Fig. 5, a comparison of the whitened region with images of the same sample acquired with the SEM is given. The whitened region, shown at 11% apparent strain in Fig. 5(a), clearly corresponds to an area exhibiting microcracks [Figs. 5(b)–5(d)] bridged by ligaments [Fig. 5(d)]. In contrast, regions that did not exhibit whitening also did not exhibit microcracks in the SEM, as is

shown in Fig. 6, where high-speed photography frames [Fig. 6(a)] showing a trabecula at different apparent strains are compared with the SEM images [Fig. 6(b)] of the same region. The trabecula seen here does not buckle or bend and is only slightly deformed even at 48% apparent strain. Correspondingly, no large microcracks (compare with Fig. 5) are visible in the SEM images.

#### IV. DISCUSSION

The differences in the mechanical properties of the three bone specimens are clearly shown in Fig. 1 and Table I. Differences in mechanical properties of bone are generally associated with sex, age and health of the donor. Bone disease, especially osteoporosis, results in an increase of fracture risk and reduced bone toughness. This parameter could be associated with the energy input needed for failure of a bone sample. In our preliminary study, this value is drastically reduced going progressively from healthy to osteoarthritic and osteoporotic bone. It should be noted, however, that quantification of the mechanical tests was subject to a systematic error; the lower support for the bone samples in the holder had two holes for fluid inlet and outlet, and thus the area of support was reduced. These holes are located close to the two front corners of the tested specimen. One of the holes can be seen in the lower left of frames of the osteoporotic sample in Fig. 2. Thus the stress values are underestimated. Because the setup was the same for all three samples, their comparison is still meaningful. In addition to the mechanical tests, the combination with high-speed photography delivered image data of the failure dynamics in real time, revealing local events. In the recorded movies it can be clearly seen that apparent strain is translated to a whole range of deformations. This result is in agreement with the work of Odgaard et al.<sup>15</sup> The retrievable data are two-dimensional, but the acquisition is much faster in contrast to other approaches delivering 3D data, which are usually combined with quasi-static tests.<sup>6,7,9–11</sup> Functional imaging of trabecular bone under load using high-speed photography can be used with a variety of strain rates. Especially high strain rates are accessible with this technique. High-speed photography has previously been applied to monitor the spiral fracture

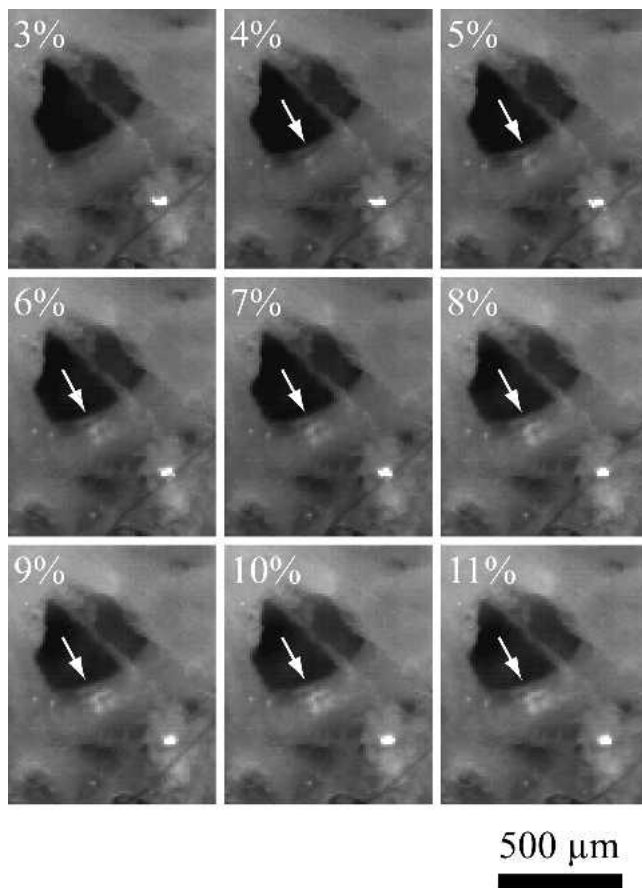


FIG. 4. Region of interest of a high-speed photography sequence of a bone sample of the healthy donor at different strains showing the progression of the whitening (arrows).

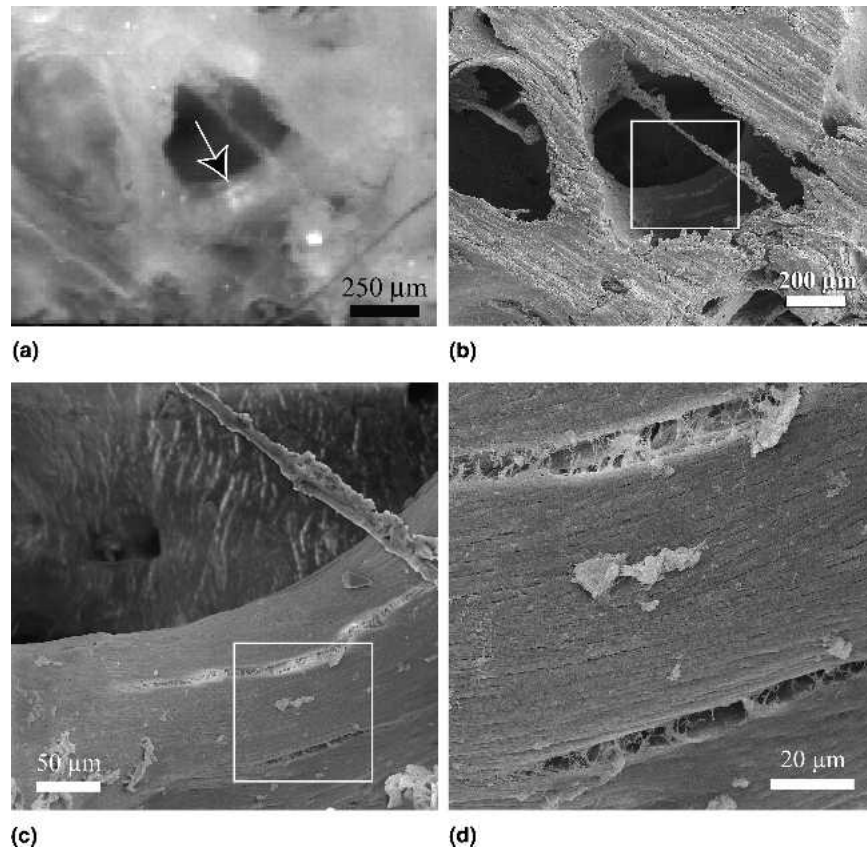


FIG. 5. Comparison between (a) high-speed photography and (b–d) SEM images of a whitened trabecula (compare Fig. 4). Two microscopic cracks spanned by ligaments can be seen in the SEM images, corresponding to the whitened region (arrow).

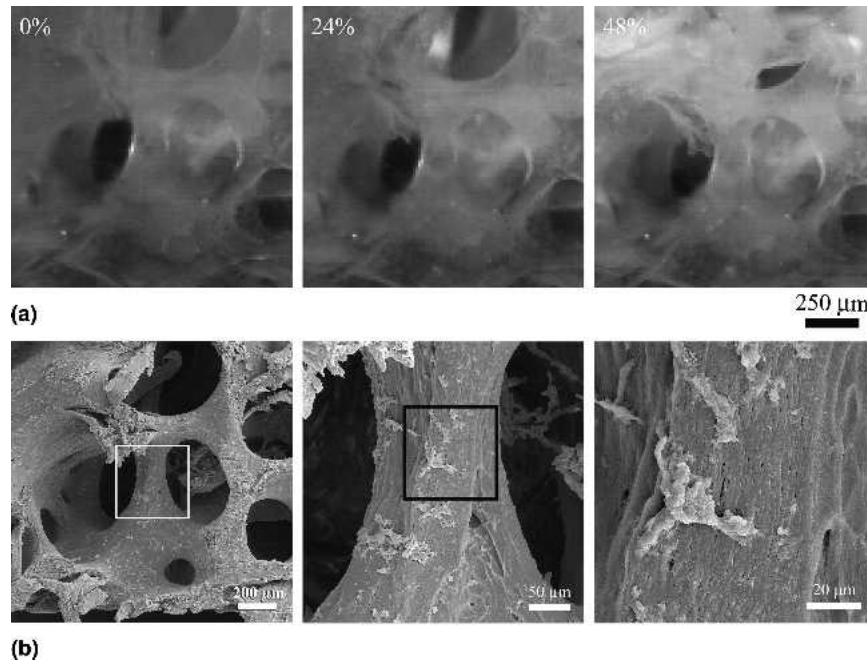


FIG. 6. Comparison between (a) high-speed photography and (b) SEM images of a trabecula that did not deform obviously and also did not exhibit any whitening. No cracks comparable to the ones shown in Fig. 5 can be seen.

of sheep femora loaded in torsion<sup>16</sup> or movements and displacements in functional spine units,<sup>17</sup> but to our best knowledge has not been used to investigate trabecular bone under compressive loads. Recorded high-speed photography frames show that deformed trabeculae whiten with increasing apparent strain. The osteoarthritic bone sample shows this effect most dramatically in this study. A region of interest where we could clearly identify bending and whitening of a trabecula was selected from these data and subjected to a motion energy filter. The filter detected elevated motion of the whitened area with increasing strain, and since the displacement pattern was not uniform, this is also an indication for elevated local strains. The whitening effect was previously hypothesized to be due to microdamage,<sup>12</sup> similar to stress whitening detected in polymers.<sup>18</sup> In a subsequent experiment on a bone sample from the previously healthy human donor, a whitened region was clearly correlated to microcracks seen in the same area using an SEM, proving the hypothesis right. It should be noted that the cracks shown in Fig. 5 are clearly not an artifact from sample preparation. In control experiments investigating a region of a similar sample, where no whitening and deformation were seen (shown in Fig. 6), as well as other samples not subjected to load (not shown), we did not find similar cracks. The smaller cracks and openings that can be seen in Fig. 6(b) are probably due to the sample preparation process but could also be caused by slight deformation experienced during the test (compressing the sample to 48% apparent strain). The microcracks found in whitened regions (compare Fig. 5) generally exhibit ligaments spanning across them in agreement with earlier studies.<sup>10,11,19,20</sup> That the whitened area in the osteoarthritic bone sample also exhibited highly elevated local strains after motion energy filtering is in agreement with the failure criterion for compact bone, where damage initiation and microdamage appear at points of highest strain.<sup>19</sup> Also, in trabecular bone it was recently found that regions exhibiting microdamage accumulation are associated with regions where high stresses and strains were predicted from finite element analyses.<sup>21</sup>

## V. CONCLUSION

In this paper, we present an exploratory study combining mechanical testing of trabecular bone with functional imaging using high-speed photography. Healthy male bone was found to have a higher elastic modulus, strength, and toughness than osteoarthritic and osteoporotic bone, with its yield point occurring at a higher apparent strain. In compressed bone, apparent strain is made up of greatly differing strains at the local level as can be seen in high-speed photography movies. Deformed trabeculae whiten, and the whitening progresses with increasing apparent and presumably also

local strain. This effect is more pronounced in the healthy and osteoarthritic bone samples than it is in the osteoporotic bone sample that we tested. Using the osteoarthritic bone sample as an example, it was shown that the whitening can be correlated with elevated displacements and qualitatively also with elevated local strains. A further study on a healthy human bone sample, using high-speed photography during compression testing and SEM, showed that the whitening is conclusively due to microcracking. Overall, high-speed photography demonstrates its value as it is noninvasive and can be simply added to a mechanical testing experiment, giving insight into failure dynamics and the possibility of detecting microcrack accumulation in real time.

## ACKNOWLEDGMENTS

We are gratefully indebted the Swiss National Science Foundation (SNF) Postdoctoral fellowship PBEZ2—105116, Austrian Science Fund (FWF) Project No. J2395-N02, Austrian Academy of Sciences (ÖAW) DOC-Fellowship, National Institute of Health (NIH) Grant No. GM65354, Veeco/DI Grant No. SB030071, Materials Research Laboratory (MRL) National Science Foundation (NSF) Grant No. DMR00-80034, North American Space Agency (NASA)/URETI Grant No. BiMAat NCC-1-02037, and the U.S. Army Research Office (Institute for Collaborative Biotechnologies) Grant No. DAAD19-030D-0004.

## REFERENCES

1. T.M. Keaveny and W.C. Hayes: A 20-year perspective on the mechanical properties of trabecular bone. *J. Biomech. Eng.* **115**, 534 (1993).
2. L.J. Melton III, E.A. Chrischilles, C. Cooper, A.W. Lane, and B.L. Riggs: Perspective. How many women have osteoporosis? *J. Bone Miner. Res.* **7**, 1005 (1992).
3. J.A. Kanis: Osteoporosis: A view into the next century. *Neth. J. Med.* **50**(5), 198 (1997).
4. R.J. McBroom, W.C. Hayes, W.T. Edwards, R.P. Goldberg, and A.A. White III: Prediction of vertebral body compressive fracture using quantitative computed tomography. *J. Bone Joint Surg. Am.* **67**, 1206 (1985).
5. M.J. Silva, T.M. Keaveny, and W.C. Hayes: Load sharing between the shell and centrum in the lumbar vertebral body. *Spine* **22**(2), 140 (1997).
6. R. Muller, S.C. Gerber, and W.C. Hayes: Micro-compression: A novel technique for the nondestructive assessment of local bone failure. *Technol. Health Care* **6**, 433 (1998).
7. B.K. Bay, T.S. Smith, D.P. Fyhrie, and M. Saad: Digital volume correlation: Three-dimensional strain mapping using x-ray tomography. *Exp. Mech.* **39**(3), 217 (1999).
8. D.P. Nicoletta, A.E. Nicholls, J. Lankford, and D.T. Davy: Machine vision photogrammetry: A technique for measurement of microstructural strain in cortical bone. *J. Biomech.* **34**(1), 135 (2001).

9. A. Nazarian and R. Muller: Time-lapsed microstructural imaging of bone failure behavior. *J. Biomech.* **37**(1), 55 (2004).
10. P. Thurner, P. Wyss, R. Voide, M. Stauber, B. Muller, M. Stampanoni, J.A. Hubell, R. Muller, and U. Sennhauser: Functional micro-imaging of soft and hard tissue using synchrotron light, in *Developments in X-Ray Tomography IV*, edited by U. Bonse (The International Society for Optical Engineering [SPIE], Bellingham, WA), Vol. 5535, pp. 112.
11. P.J. Thurner, P. Wyss, R. Voide, M. Stauber, M. Stampanoni, U. Sennhauser, and R. Muller: Time-lapsed investigation of three-dimensional failure and damage accumulation in trabecular bone using synchrotron light. *Bone* (2006, in press).
12. J.D. Currey: *Bones: Structure and Mechanics* (Princeton University Press, Princeton, NJ, 2002).
13. B.K. Bay: Texture correlation: a method for the measurement of detailed strain distributions within trabecular bone. *J. Orthop. Res.* **13**(2), 258 (1995).
14. E.H. Adelson and J.R. Bergen: Spatiotemporal energy models for the perception of motion. *J. Opt. Soc. Am. A, Opt. Image Sci. Vis.* **2**(2), 284 (1985).
15. A. Odgaard, I. Hvid, and F. Linde: Compressive axial strain distributions in cancellous bone specimens. *J. Biomech.* **22**, 829 (1989).
16. W. Bonfield and M.D. Grynbas: Spiral fracture of cortical bone. *J. Biomech.* **15**, 555 (1982).
17. A.L. Osvalder, P. Neumann, P. Lovsund, and A. Nordwall: A method for studying the biomechanical load response of the (in-vitro) lumbar spine under dynamic flexion shear loads. *J. Biomech.* **26**, 1227 (1993).
18. B.W. Cherry and T.S. Hin: Stress whitening in polyethylene. *Polymer* **22**, 1610 (1981).
19. R.K. Nalla, J.H. Kinney, and R.O. Ritchie: Mechanistic fracture criteria for the failure of human cortical bone. *Nat. Mater.* **2**(3), 164 (2003).
20. G.E. Fantner, T. Hassenkam, J.H. Kindt, J.C. Weaver, H. Birkedal, L. Pechenik, J.A. Cutroni, G.A.G. Cidade, G.D. Stucky, D.E. Morse, and P.K. Hansma: Sacrificial bonds and hidden length dissipate energy as mineralized fibrils separate during bone fracture. *Nature Mater.* **4**, 612 (2005).
21. S. Nagaraja, T.L. Couse, and R.E. Guldberg: Trabecular bone microdamage and microstructural stresses under uniaxial compression. *J. Biomech.* **38**, 707 (2005).